Available online at www.sciencedirect.com
SCIENCE DIRECT
C. R. Mecanique 333 (2005) 413–418
COMPTES RENDUS MECANIQUE
http://france.elsevier.com/direct/CRAS2B/

# Settling motion of interacting solid particles in the vicinity of a plane solid boundary

Antoine Sellier

*LadHyX, École polytechnique, 91128 Palaiseau cedex, France*

Received 5 November 2004; accepted after revision 14 February 2005

Available online 8 April 2005

Presented by Évariste Sanchez-Palencia

**Abstract**

The sedimentation of $N \geqslant 1$ small arbitrarily-shaped solid bodies near a solid plane is addressed by discarding inertial effects and using $6N$ boundary-integral equations. Numerical results for 2 or 3 identical spheres reveal that combined wall–particle and particle–particle interactions deeply depend on the cluster's geometry and distance to the wall and may even cancel for a sphere which then moves as it were isolated. ***To cite this article: A. Sellier, C. R. Mecanique 333 (2005).***


**Résumé**

**Sédimentation d'un ensemble de particules solides en présence d'une paroi solide plane.** La sédimentation en régime de Stokes de $N \geqslant 1$ corps solides quelconques situés près d'une paroi plane est étudiée à l'aide de $6N$ équations de frontière. Les résultats pour 2 ou 3 sphères identiques montrent que la résultante des intéractions particule-particule et paroi-particule est très sensible à la disposition des sphères et peut même s'annuler pour l'une d'elles qui dans ce cas migre comme si elle était seule. ***Pour citer cet article : A. Sellier, C. R. Mecanique 333 (2005).***


*Keywords:* Fluid mechanics; Sedimentation; Particle–particle interactions; Wall–particle interactions; Boundary elements

*Mots-clés :* Mécanique des fluides ; Sédimentation ; Interactions particule-particule ; Interactions particule-paroi ; Eléments de frontière

## 1. Introduction

The new approach advocated in [1] to compute the low-Reynolds-number falling motions of $N \geqslant 1$ arbitrarily-shaped solid bodies investigates pure particle–particle interactions in sedimentation. However, boundaries are also

*E-mail address:* sellier@ladhyx.polytechnique.fr (A. Sellier).

1631-0721/$ – see front matter 
doi:10.1016/j.crme.2005.02.008

encountered in practice and the case of a solid wall has been only handled in [2,3] for $N = 1$ and for several spheres in axisymmetric motion in [4]. The present work thus investigates combined particle–particle and wall–particle interactions for arbitrary clusters lying near a plane solid wall $\Sigma$ by extending [1]. This is achieved by using this time a Green's tensor [5] that vanishes on $\Sigma$ and therefore again solving $6N$ boundary-integral equations on the entire cluster's surface.

## 2. Governing linear system

We look at $N \geqslant 1$ solid arbitrarily-shaped particle(s) $\mathcal{P}_n$ $(n = 1, \ldots, N)$ immersed in a Newtonian fluid of uniform viscosity $\mu$ and density $\rho$ above the solid and motionless $x_3 = 0$ plane $\Sigma$. For example, the case of a few spheres is sketched in Fig. 1.

Under the uniform gravity $\mathbf{g}$ each $\mathcal{P}_n$ with center of mass $O_n$ settles with respect to the Cartesian frame $(O, x_1, x_2, x_3)$ at the unknown angular velocity $\boldsymbol{\Omega}^{(n)}$ and translational velocity $\mathbf{U}^{(n)}$ (the velocity of $O_n$). The fluid and each $\mathcal{P}_n$ with volume $\mathcal{V}_n$, center of volume $O'_n$, mass $\mathcal{M}_n$ and surface $S_n$ have negligible inertia. Hence, the liquid has at a current point $M$ quasi-steady [1] velocity $\mathbf{u}$, pressure $p + \rho\mathbf{g} \cdot \mathbf{OM}$ and stress tensor $\boldsymbol{\sigma}$ that obey

$$\mu\nabla^2\mathbf{u} = \nabla p \quad \text{and} \quad \nabla \cdot \mathbf{u} = 0 \quad \text{in } \Omega, \quad (\mathbf{u}, p) \to (\mathbf{0}, 0) \quad \text{as } |\mathbf{OM}| \to \infty \tag{1}$$

$$\mathbf{u} = \mathbf{0} \quad \text{on } \Sigma \quad \text{and} \quad \mathbf{u} = \mathbf{U}^{(n)} + \boldsymbol{\Omega}^{(n)} \wedge \mathbf{O_nM} \quad \text{on } S_n \quad (n \geqslant 1) \tag{2}$$

$$\int_{S_n} \boldsymbol{\sigma} \cdot \mathbf{n}\,\mathrm{d}S_n + (M_n - \rho\mathcal{V}_n)\mathbf{g} = \mathbf{0}, \qquad \int_{S_n} \mathbf{O_nM} \wedge \boldsymbol{\sigma} \cdot \mathbf{n}\,\mathrm{d}S_n + \rho\mathcal{V}_n\mathbf{g} \wedge \mathbf{O_nO'_n} = \mathbf{0} \quad (n \geqslant 1) \tag{3}$$

with $\Omega$ the fluid domain and $\mathbf{n}$ the unit outward normal on the cluster's surface $S = \bigcup_{n=1}^{N} S_n$. In order to rewrite (3), that requires zero net force and torque (with respect to $O_n$) on each $\mathcal{P}_n$ of ignored inertia, let us introduce $6N$ flows $(\mathbf{u}_L^{(n),i}, p_L^{(n),i})$ with stress tensor $\boldsymbol{\sigma}_L^{(n),i}$ for $L \in \{T, R\}, i \in \{1, 3\}$ and $n = 1, \ldots, N$. Those flows fulfill (1) and the conditions

$$\mathbf{u}_L^{(n),i} = \mathbf{0} \quad \text{on } \Sigma, \quad \mathbf{u}_L^{(n),i} = \mathbf{0} \quad \text{on } S_m \text{ if } m \neq n, \qquad \mathbf{u}_T^{(n),i} = \mathbf{e}_i \quad \textit{and} \quad \mathbf{u}_R^{(n),i} = \mathbf{e}_i \wedge \mathbf{O_nM} \quad \text{on } S_n \tag{4}$$

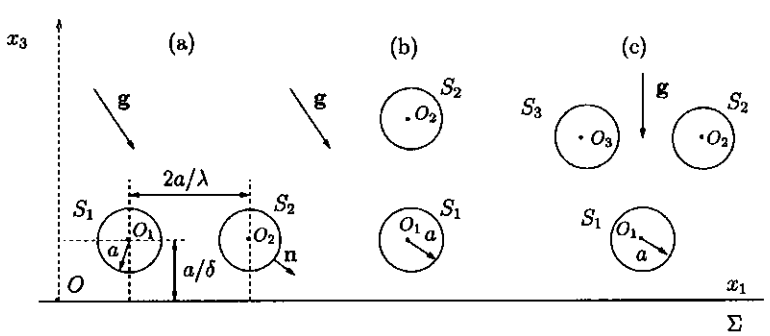


Fig. 1. Identical spheres near the $x_3 = 0$ solid plane $\Sigma$: (a) 2-sphere cluster with $\mathbf{O_1O_2} \cdot \mathbf{e}_3 = 0$; (b) 2-sphere cluster with $\mathbf{O_1O_2}$ normal to $\Sigma$; (c) 3-sphere cluster with $O_1O_2 = O_1O_3 = O_2O_3$, $\mathbf{O_2O_3} \cdot \mathbf{e}_3 = 0$ and $\mathbf{g} = -g\mathbf{e}_3$.

Fig. 1. Sphères identiques au voisinage du plan solide $\Sigma$ $(x_3 = 0)$ : (a) $N = 2$ et $\mathbf{O_1O_2} \cdot \mathbf{e}_3 = 0$ ; (b) $N = 2$ et $\mathbf{O_1O_2}$ perpendiculaire à $\Sigma$ ; (c) $N = 3$ et $O_1O_2 = O_1O_3 = O_2O_3$, $\mathbf{O_2O_3} \cdot \mathbf{e}_3 = 0$, $\mathbf{g} = -g\mathbf{e}_3$.

Because $\mathbf{u} = \mathbf{0}$ on $\Sigma$ where $\mathbf{n} = \mathbf{e}_3$ the usual reciprocal identity [6] provides, for any flow $(\mathbf{u}', p')$ with stress tensor $\boldsymbol{\sigma}'$ satisfying the equations and far-field behavior (1), the relation

$$\int_{S\cup\Sigma} \mathbf{u}' \cdot \boldsymbol{\sigma} \cdot \mathbf{n}\,\mathrm{d}S = \int_{S\cup\Sigma} \mathbf{u} \cdot \boldsymbol{\sigma}' \cdot \mathbf{n}\,\mathrm{d}S = \sum_{m=1}^{N} \int_{S_m} \mathbf{u} \cdot \boldsymbol{\sigma}' \cdot \mathbf{n}\,\mathrm{d}S_m \tag{5}$$

Upon introducing the vector $\mathbf{f}_L^{(n),i} = \boldsymbol{\sigma}_L^{(n),i} \cdot \mathbf{n}$ on $S$, the quantities $A_{(m),L}^{(n),i,j}$ and $B_{(m),L}^{(n),i,j}$ with

$$A_{(m),L}^{(n),i,j} = -\int_{S_m} \mathbf{e}_j \cdot \mathbf{f}_L^{(n),i}\,\mathrm{d}S_m, \qquad B_{(m),L}^{(n),i,j} = -\int_{S_m} (\mathbf{e}_j \wedge \mathbf{O_m M}) \cdot \mathbf{f}_L^{(n),i}\,\mathrm{d}S_m \tag{6}$$

and adopting henceforth the tensor summation convention with $\mathbf{U}^{(n)} = U_j^{(n)}\mathbf{e}_j$ and $\boldsymbol{\Omega}^{(n)} = \Omega_j^{(n)}\mathbf{e}_j$, the choice $(\mathbf{u}', p') = (\mathbf{u}_L^{(n),i}, p_L^{(n),i})$ in (5) easily shows that (3) becomes

$$\{A_{(m),T}^{(n),i,j} U_j^{(m)} + B_{(m),T}^{(n),i,j} \Omega_j^{(m)}\}\mathbf{e}_i = (\mathcal{M}_n - \rho\mathcal{V}_n)\mathbf{g} = \mathbf{T}^{(n)} \tag{7}$$

$$\{A_{(m),R}^{(n),i,j} U_j^{(m)} + B_{(m),R}^{(n),i,j} \Omega_j^{(m)}\}\mathbf{e}_i = \rho\mathcal{V}_n(\mathbf{g} \wedge \mathbf{O_n O'_n}) \cdot \mathbf{e} = \mathbf{C}^{(n)} \tag{8}$$

Setting $\mathbf{Y} = (\mathbf{T}^{(1)}, \ldots, \mathbf{T}^{(N)}, \mathbf{C}^{(1)}, \ldots, \mathbf{C}^{(N)})$, the linear system (7), (8) with $6N \times 6N$ matrix $\mathbf{A}$ also reads $\mathbf{A} \cdot {}^t\mathbf{X} = {}^t\mathbf{Y}$ with $\mathbf{X} = (\mathbf{U}^{(1)}, \ldots, \mathbf{U}^{(N)}, \boldsymbol{\Omega}^{(1)}, \ldots, \boldsymbol{\Omega}^{(N)})$ the unknown generalized velocity and ${}^t\mathbf{V}$ the transposed of $\mathbf{V}$. As seen by putting $(\mathbf{u}, p) = (\mathbf{u}_L^{(n),i}, p_L^{(n),i})$ and $(\mathbf{u}', p') = (\mathbf{u}_L^{(m),j}, p_L^{(m),j})$ in the first equality (5) the matrix $\mathbf{A}$ is symmetric. Moreover, if $\nabla[\mathbf{u} \cdot \mathbf{e}_i] = \nabla[u_i] = u_{i,j}\mathbf{e}_j$ and $e_{ij} = (u_{i,j} + u_{j,i})/2$, the divergence theorem and (1) yield

$$E := \int_{S\cup\Sigma} \mathbf{u} \cdot \boldsymbol{\sigma} \cdot \mathbf{n}\,\mathrm{d}S = -2\mu \int_{\Omega} e_{ij}e_{ij}\,\mathrm{d}\Omega < 0 \tag{9}$$

Since (2) and (4) show that $\boldsymbol{\sigma} \cdot \mathbf{n} = U_i^{(n)}\mathbf{f}_T^{(n),i} + \Omega_i^{(n)}\mathbf{f}_R^{(n),i}$ on $S$ and $\mathbf{u} = U_j^{(m)}\mathbf{e}_j + \Omega_j^{(m)}(\mathbf{e}_j \wedge \mathbf{O_m M})$ on $S_m$ it follows from (9), (2) and (6) that $E = -\mathbf{X} \cdot \mathbf{A} \cdot {}^t\mathbf{X} < 0$ whatever $\mathbf{X}$. Hence, $\mathbf{A}$ is not only real-valued and symmetric but also positive-definite and (7), (8) thus admit a unique solution $\mathbf{X}$, here obtained (see (6)) by solely evaluating the surface tractions $\mathbf{f}_L^{(n),i}$ on the multiply-connected (if $N \geqslant 2$) cluster's boundary $S$.

## 3. Relevant integral representations and boundary-integral equations

We denote by $M'(x_1, x_2, -x_3)$ the symmetric with respect to the plane $\Sigma$ of any point $M(x_1, x_2, x_3)$ located in $\Omega \cup S \cup \Sigma$ and introduce for $P$ on $S$ the pseudo-functions [5]

$$G_{jk}^0(P, M) = \delta_{jk}/PM + (\mathbf{PM} \cdot \mathbf{e}_j)(\mathbf{PM} \cdot \mathbf{e}_k)/PM^3 \tag{10}$$

$$G_{jk}^1(P, M) = -G_{jk}^0(P, M') - 2c_j\big[(\mathbf{OM} \cdot \mathbf{e}_3)/PM'^3\big]\big\{\delta_{k3}\mathbf{PM}' \cdot \mathbf{e}_j - \delta_{j3}\mathbf{PM}' \cdot \mathbf{e}_k + \mathbf{OP} \cdot \mathbf{e}_3\big[\delta_{jk} - 3(\mathbf{PM}' \cdot \mathbf{e}_j)(\mathbf{PM}' \cdot \mathbf{e}_k)/PM'^2\big]\big\} \tag{11}$$

with $c_1 = c_2 = 1$, $c_3 = -1$ and $\delta_{jk}$ the Kronecker delta. Extending in our case $N \geqslant 1$ the result obtained in [7,8] for a single particle it is found that $\mathbf{u}_L^{(n),i}$, subject to (1) and (4), then admits the key single-layer integral representation

$$-8\pi\mu[\mathbf{u}_L^{(n),i} \cdot \mathbf{e}_j](M) = \int_S \big[G_{jk}^0 + G_{jk}^1\big](P, M)\big[\mathbf{f}_L^{(n),i}(P) \cdot \mathbf{e}_k\big]\mathrm{d}S \quad \text{for } M \text{ in } \Omega \cup S \cup \Sigma \tag{12}$$

The above key result (12) appeals to the following remarks and basic consequences:

(i) Of course $\mathbf{u}_L^{(n),i}$ vanishes on $\Sigma$ because $[G_{jk}^0 + G_{jk}^b](P, M) = 0$ if $M$ lies on $\Sigma$ [5]. However, (12) in general also involves for $(\mathbf{u}'', p'')$ subject to (1) and the property $\mathbf{u}'' = \mathbf{0}$ on $\Sigma$ an additional double-layer integral which only vanishes if $\mathbf{u}''$ is a rigid-body motion on each $S_m$ (as is each $\mathbf{u}_L^{(n),i}$).

(ii) Each unknown traction $\mathbf{f}_L^{(n),i}$ obeys on $S$ a Fredholm boundary-integral equation of the first kind obtained by combining (4) and (12). One thus determines $\mathbf{X} = (\mathbf{U}^{(1)}, \ldots, \mathbf{U}^N, \boldsymbol{\Omega}^{(1)}, \ldots, \boldsymbol{\Omega}^{(N)})$ by solving $6N$ integral equations on the cluster's surface.

(iii) Once all vectors $\mathbf{f}_L^{(n),i}$ and $\mathbf{X}$ have been evaluated, (12) finally provides if necessary the velocity fields $\mathbf{u}_L^{(n),i}$ and therefore $\mathbf{u} = U_i^{(n)} \mathbf{u}_L^{(n),i} + \Omega_i^{(n)} \mathbf{u}_R^{(n),i}$ in the liquid domain $\Omega$.

## 4. Numerical method and preliminary results

As in [1], the integral equation (12) for $\mathbf{f}_L^{(n),i}$ is inverted by a boundary element technique [9] with 6-node isoparametric curved triangular elements and $N_m$ nodes on each $S_m$ and a $LU$ factorization algorithm to solve the discretized counterpart of (12). The procedure which readily recovers [1] far from the wall (see (10), (11)) is tested for a single spheroid with uniform density $\rho_s$, inequation $x_1^2 + x_2^2 + \epsilon^{-2}(x_3 - H)^2 / \leqslant a^2$ and separation ratio $h = H/(\epsilon a) > 1$. If isolated ($h = \infty$) this body only translates for $\mathbf{g} = g\mathbf{e}_3$ at the velocity $\mathbf{U}^{(1)} = ga^2(\rho_s - \rho)v(\epsilon)/\mu\mathbf{e}_3$ with $v(1) = 2/9$ for a sphere and for oblate spheroids [6]

$$v(\epsilon) = \left\{p(p^2+3)\arctan(1/p) - p^2\right\}/12 \quad \text{with } p = \epsilon/(1-\epsilon^2)^{1/2} \text{ and } 0 < \epsilon < 1 \tag{13}$$

Symmetries and linearity confine the analysis to the settings $\mathbf{g} = g\mathbf{e}_1$ and $\mathbf{g} = -g\mathbf{e}_3$ with $g > 0$. For $\rho_s \neq \rho$ the non-zero Cartesian velocities, normalized by the velocity of the isolated spheroid and solely depending upon $(\epsilon, h)$, are found to be

$$u_1 = \frac{\mu a^{-2}\mathbf{U}^{(1)} \cdot \mathbf{e}_1}{g(\rho_s - \rho)v(\epsilon)}, \quad w_2 = \frac{\mu a^{-3}\boldsymbol{\Omega}^{(1)} \cdot \mathbf{e}_2}{g(\rho_s - \rho)v(\epsilon)} \quad \text{if } \mathbf{g} = g\mathbf{e}_1; \quad u_3 = \frac{\mu a^{-2}\mathbf{U}^{(1)} \cdot \mathbf{e}_3}{g(\rho - \rho_s)v(\epsilon)} \quad \text{if } \mathbf{g} = -g\mathbf{e}_3 \tag{14}$$

The computed values are compared in Table 1, for different $N_1$-node meshes on $S_1$, both with the analytical bipolar coordinates method [10] for a sphere ($\epsilon = 1$) and the numerical results of [3] for the $\epsilon = 1/2$ oblate spheroid.

Clearly, the agreement is excellent for the sphere and very good for the oblate spheroid. Actually, [2,3] kept in (12) the extra weakly-singular double-layer integral although (remind our remark (i) below (12)) it vanishes and this might explain the small observed discrepancies for $\epsilon = 1/2$.

Although the advocated procedure holds for $N \geqslant 1$ arbitrary bodies, we henceforth present results for clusters (see Fig. 1) of 2 or 3 identical spheres $\mathcal{P}_n$ with center $O_n$, radius $a$ and uniform density $\rho_s \neq \rho$. We put 242 nodes

Table 1
Computed normalized velocities $u_1$, $w_2$ and $u_3$ (see (14)) for a sphere ($\epsilon = 1$) and the $\epsilon = 1/2$ oblate spheroid for different $N_1$-node meshes

Tableau 1
Vitesses adimensionnées $u_1$, $w_2$ and $u_3$ (voir (14)) pour une sphère ($\epsilon = 1$) et un ellipsoide de révolution aplati ($\epsilon = 1/2$) en fonction du nombre $N_1$ de points de collocation

| $N_1$ | $h$ | $u_1; \epsilon = 1$ | $w_2; \epsilon = 1$ | $u_3; \epsilon = 1$ | $u_1; \epsilon = 0.5$ | $w_2; \epsilon = 0.5$ | $u_3; \epsilon = 0.5$ |
|---|---|---|---|---|---|---|---|
| 74 | 1.1 | 0.4463 | 0.0245 | 0.1087 | 0.6433 | −0.0534 | 0.246 |
| 242 | 1.1 | 0.4424 | 0.0259 | 0.0886 | 0.6413 | −0.0538 | 0.244 |
| 1058 | 1.1 | 0.4430 | 0.0270 | 0.0871 | 0.6411 | −0.0538 | 0.244 |
| [10, 3] | 1.1 | 0.4430 | 0.0270 | 0.0873 | 0.6464 | −0.0522 | 0.241 |
| 74 | 2.0 | 0.7256 | 0.0034 | 0.4726 | 0.7910 | −0.0250 | 0.473 |
| 242 | 2.0 | 0.7235 | 0.0035 | 0.4707 | 0.7890 | −0.0252 | 0.472 |
| 1058 | 2.0 | 0.7232 | 0.0035 | 0.4705 | 0.7888 | −0.0252 | 0.472 |
| [10, 3] | 2.0 | 0.7232 | 0.0035 | 0.4705 | 0.7892 | −0.0252 | 0.477 |

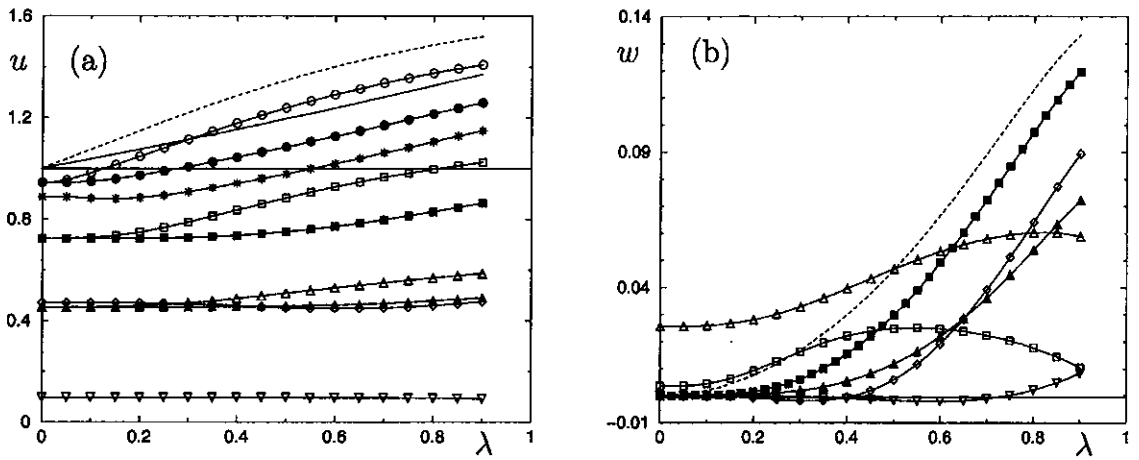


Fig. 2. Normalized velocities $u$ and $w$ in Cases k if $N = 2$ and $\mathbf{O_1O_2} \cdot \mathbf{e}_3 = 0$ for $\delta = 0.1$ ($k = 1(\circ), k = 2(\bullet), k = 3(*)$), $\delta = 0.5$ ($k = 1(\square)$, $k = 2(\blacksquare), k = 3(\diamond)$) and $\delta = 0.9$ ($k = 1(\triangle), k = 2(\blacktriangle), k = 3(\triangledown)$). (a) $u$ with dashed ($k = 1, 2$) and solid ($k = 3$) curves for $\delta = 0$; (b) $w$ with dashed ($k = 2, 3$) and solid ($k = 1$) curves for $\delta = 0$.

Fig. 2. Vitesses adimensionnées $u$ et $w$ dans les Cas k si $N = 2$ et $\mathbf{O_1O_2} \cdot \mathbf{e}_3 = 0$ pour $\delta = 0.1(k = 1(\circ), k = 2(\bullet), k = 3(*))$, $\delta = 0.5$ ($k = 1(\square), k = 2(\blacksquare), k = 3(\diamond)$) et $\delta = 0.9$ ($k = 1(\triangle), k = 2(\blacktriangle), k = 3(\triangledown)$). (a) $u$ avec des courbes en trait pointillé ($k = 1, 2$) et plein ($k = 3$) pour $\delta = 0$ ; (b) $w$ avec des courbes en trait pointillé ($k = 2, 3$) et plein ($k = 1$) pour $\delta = 0$.

on $S_n$ and introduce the positive wall–sphere and sphere–sphere separation parameters as $\delta = a/\mathbf{OO_1} \cdot \mathbf{e}_3 < 1$ and $\lambda = 2a/O_1O_2 < 1$, respectively. By linearity we consider the settings $\mathbf{g} = g\mathbf{e}_1$ (Case 1), $\mathbf{g} = g\mathbf{e}_2$ (Case 2), $\mathbf{g} = -g\mathbf{e}_3$ (Case 3) with $g > 0$ and use in Case k the normalized velocities

$$u_i^{(n),(k)} = \frac{9\mu a^{-2}\mathbf{U}^{(n)} \cdot \mathbf{e}_i}{2g(\rho_s - \rho)c_k}, \quad w_i^{(n),(k)} = \frac{9\mu a^{-3}\boldsymbol{\Omega}^{(n)} \cdot \mathbf{e}_i}{2g(\rho_s - \rho)c_k} \quad \text{with } c_1 = c_2 = 1,\ c_3 = -1 \tag{15}$$

For 2 spheres and $\mathbf{O_1O_2} \cdot \mathbf{e}_3 = 0$ (see Fig. 1(a)) only $u = u_k^{(1),(k)} = u_k^{(2),(k)}$ in each Case k, $w = w_2^{(1),(1)} = w_2^{(2),(1)}$ in Case 1, $w = w_3^{(1),(2)} = -w_3^{(2),(2)}$ in Case 2 and $w = w_2^{(1),(3)} = -w_2^{(2),(3)}$ in Case 3 are non-zero. These quantities are plotted in Fig. 2 versus $\lambda$.

As seen in Fig. 2(a), pure wall–sphere ($\lambda = 0$) interactions slow down the spheres ($u < 1$) and increase with $\delta$ and pure sphere–sphere ($\delta = 0$) interactions speed up the spheres ($u > 1$) and increase with $\lambda$. For $\delta\lambda \neq 0$ both interactions interact and $u - 1$ deeply depends on $(\delta, \lambda)$. If $\delta = 0.1$ (all Cases k) and $\delta = 0.5$ (Case 1) we may have $u = 1$ (a sphere ignores the other one and $\Sigma$) or also $u > 1$ if $\lambda$ and $\delta$ are large and small enough, respectively. In other cases wall–particle interactions are dominant and spheres move slower than if isolated ($u < 1$). This actually occurs near the wall whatever $\lambda$ since $u$ then weakly depends on $\lambda$, as observed for $\lambda = 0.9$. Finally, note that $u$ strongly depends on Case k and $u_1^{(1),(1)} > u_2^{(1),(2)} > u_3^{(1),(3)}$ for any pair $(\delta, \lambda)$ with $\delta\lambda \neq 0$. In Fig. 2(b) similar trends are obtained for $w$ with $w_3^{(1),(2)} > w_2^{(1),(3)}$ and $w \to 0$ as $\lambda \to 1$ in Case 1 (not in Cases 2 or 3).

If $\mathbf{O_1O_2}$ is normal to $\Sigma$ (see Fig. 1(b)) non-zero velocities read $u(n) = u_1^{(n),(1)} = u_2^{(n),(2)}$ in Case 1 (or 2) and $u(n) = u_3^{(n),(3)}$ in Case 3. As depicted in Fig. 3(a), $u(1) < u(2)$ in each Case k for $\delta > 0$ since $\mathcal{P}_1$ experiences stronger wall–sphere interactions than $\mathcal{P}_2$. As in Fig. 2(a), $u(n)$ decreases as $\delta$ increases for any $\lambda$ and $\mathcal{P}_n$ might ignore the other sphere ($u(n) = 1$) for $(n, \delta) = (1, 0.3)$ in Case 1 and $(n, \delta) = (2, 0.3)$ in Cases 1, 3. In addition, $u(n)$ is smaller in Case 3 than in Case 1 and $u(2)$ strongly decreases as $\lambda$ increases for $\delta = 0.9$.

Finally, we consider in Case 3 the 3-sphere cluster sketched in Fig. 1(c) by plotting in Fig. 3(b) the velocities $u(n) = u_3^{(n),(3)}$ for $10\lambda = 1, 5, 9$. Clearly, $u(1)$ and $u(2) = u(3)$ decrease with $1/\delta$ or $\lambda$ and for a given sphere–sphere separation $\lambda$ there exist wall positions $\delta_1$ such that $u(1) = 1$, $\delta_2$ such that $u(2) = 1$ and $\delta_c$ at which all spheres adopt the same velocity ($u(1) = u(2) > 1$) whereas $u(2) - u(1)$ has sign of $\delta - \delta_c$ for $\delta \neq \delta_c$.

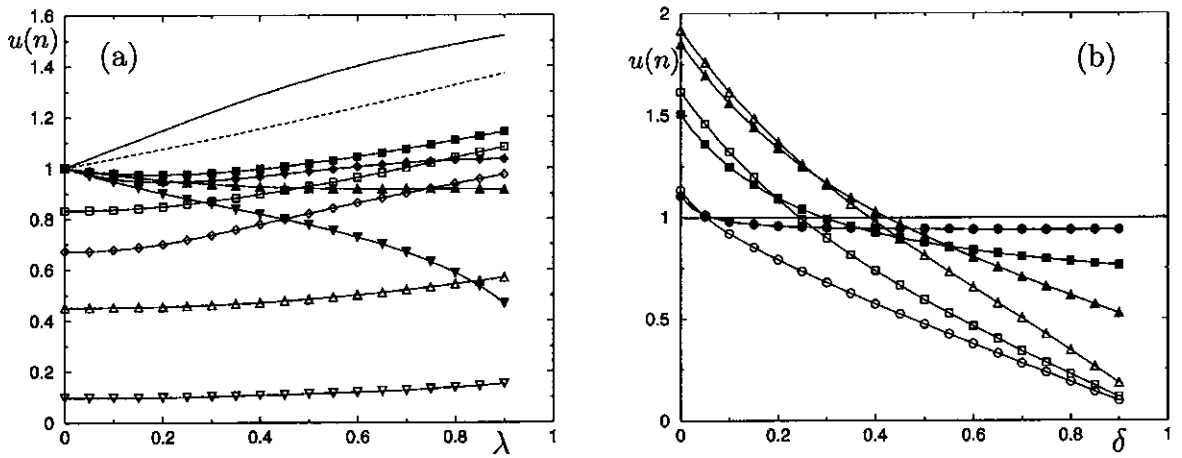


Fig. 3. (a) Normalized velocities $u(n)$ for $N = 2$ and $\mathbf{O_1O_2}$ normal to $\Sigma$ in Case 1 for $\delta = 0.3$ ($n = 1(\square), n = 2(\blacksquare)$) or $\delta = 0.9$ ($n = 1(\triangle), n = 2(\blacktriangle)$) and in Case 3 for $\delta = 0.3$ ($n = 1(\Diamond), n = 2(\blacklozenge)$) or $\delta = 0.9$ ($n = 1(\triangledown), n = 2(\blacktriangledown)$); (b) velocities $u(n)$ versus $\delta$ for $N = 3$ in Case 3 if $\lambda = 0.1$ ($n = 1(\circ), n = 2(\bullet)$), $\lambda = 0.5$ ($n = 1(\square), n = 2(\blacksquare)$) and $\lambda = 0.9$ ($n = 1(\triangle), n = 2(\blacktriangle)$).

Fig. 3. (a) Vitesses adimensionnées $u(n)$ si $N = 2$ et $\mathbf{O_1O_2}$ normal à $\Sigma$ dans le Cas 1 pour $\delta = 0.3$ ($n = 1(\square), n = 2(\blacksquare)$) ou $\delta = 0.9$ ($n = 1(\triangle), n = 2(\blacktriangle)$) et dans le Cas 3 pour $\delta = 0.3$ ($n = 1(\Diamond), n = 2(\blacklozenge)$) ou $\delta = 0.9$ ($n = 1(\triangledown), n = 2(\blacktriangledown)$) ; (b) vitesses $u(n)$ dans le Cas 3 si $N = 3$ et $\lambda = 0.1$ ($n = 1(\circ), n = 2(\bullet)$), $\lambda = 0.5$ ($n = 1(\square), n = 2(\blacksquare)$) ou $\lambda = 0.9$ ($n = 1(\triangle), n = 2(\blacktriangle)$).

## 5. Conclusions

The proposed procedure has a reasonable cpu-time cost and may therefore be embedded in a Runge–Kutta march-in-time algorithm to track a time-dependent cluster's geometry as time evolves. This task is under investigation both for spheres and non-spherical bodies. As obtained in [3] for one spheroid, we expect to find equilibrium orientations of non-spherical particles for a few specific initial clusters.

## References

[1] A. Sellier, On the slow gravity-driven migration of arbitrary clusters of small solid particles, C. R. Mécanique 332 (12) (2004) 987–992.
[2] R. Hsu, P. Ganatos, The motion of a rigid body in viscous fluid bounded by a plane wall, J. Fluid Mech. 207 (1989) 29–72.
[3] L. Elasmi, M. Berzig, F. Feuillebois, Stokes flow for the axisymmetric motion of several spherical particles perpendicular to a plane wall, Z. Angew. Math. Phys. 54 (2003) 1–24.
[4] R. Hsu, P. Ganatos, Gravitational and zero-drag motion of a spheroid adjacent to an inclined plane at low Reynolds number, J. Fluid Mech. 268 (1994) 267–292.
[5] J.R. Blake, A note on the image system for a Stokeslet in a no-slip boundary, Proc. Cambridge Philos. Soc. 70 (1971) 303–310.
[6] J. Happel, H. Brenner, Low Reynolds Number Hydrodynamics, Martinus Nijhoff, 1973.
[7] C. Pozrikidis, Boundary Integral and Singularity Methods for Linearized Viscous Flow, Cambridge University Press, 1992.
[8] E. Gavze, M. Shapiro, Particles in a shear flow near a solid wall: effect of nonsphericity on forces and velocities, Int. J. Multiphase Flow 23 (1) (1997) 155–182.
[9] M. Bonnet, Boundary Integral Equation Methods for Solids and Fluids, Wiley, 1999.
[10] M. Chaoui, F. Feuillebois, Creeping flow around a sphere in shear flow close to a wall, Q. J. Mech. Appl. Math. 56 (2003) 381–410.